A Prototype DSN X-S Band Feed: DSS 13 Application Status (Third Report)

W. Williams, D. Nixon, H. Reilly, J. Withington, and D. Bathker
Radio Frequency and Microwave Subsystems Section

This article, the third in this series discussing a new prototype X-S band horn feed for future use at various DSN sites, deals with the testing of the final fabricated feed at DSS 13. Measured feedhorn patterns are presented and efficiencies calculated. Preliminary results of system noise temperature and 26-m antenna system gain measurements are presented. Also discussed are some measurements leading to an improved second generation feed.

The preliminary results of the field measurements indicate that this horn will perform as originally specified and required. Also the tests for the second generation feed have indicated the potential cause of minor X-band moding.

I. Introduction

The first report (Ref. 1) of this series discusses the design of a dual-band (X-S) corrugated horn for DSN applications. The radiation patterns and efficiencies of a half-scale model were presented in Ref. 1. The second report (Ref. 2) discusses the design of a diplexer or X-S combiner for injecting signals into the horn. A combiner for the X-S horn was fabricated. Also, efficiency calculations were made for the half-scale model horn patterns scattered from the Venus (DSS 13) site subreflector.

The final full-scale horn fabrication has been completed, and full-scale measurements were made. These measurements indicate some additional problems in hybrid moding, which must be resolved. The full-scale horn was assembled in a feedcone with other electronic equipment and shipped to the DSS 13 site, where preliminary temperature measurements were made at X-band frequencies. The cone was mounted on the 26-m antenna for final evaluation.

The final full-scale horn pattern measurements were used in the JPL theoretical scattering program (Ref. 3) to determine final efficiencies after reflection from the DSS 13 site hyperboloid with vertex plate. The program (spherical wave expansion) takes into account the fact that the subreflector is at a range somewhat less than D^2/λ.

II. The Final X-S Horn

The final Phase I X-S horn is shown in Fig. 1, and measured radiation patterns of this horn are shown in Figs. 2, 3, and 4. Although these patterns are acceptable, there are some

differences from the measured half-scale model at frequencies in the high end of the X-band region (Fig. 2). There is a marked difference in the E and H plane patterns, the E plane being broader with a 1-dB null (or dip) on axis. This results in more forward spillover from this broader E-plane pattern, and a somewhat reduced efficiency.

The E and H plane patterns (Fig. 3) at 7.175 GHz overlay much better, although there is evidence of some difference near boresight where slight dips occur. Figure 4 indicates a slight difference in the E and H plane patterns at 2.295 GHz, but so minor as to be ignored.

It is next necessary to predict the final RF efficiency of DSS 13 with this feedhorn in place. This is done by decomposing the patterns into Fourier-type components using the spherical wave expansion technique of Ref. 3. These components are then used to determine currents upon the DSS 13 subreflector at the proper range from the horn and hence determine the final scattered pattern that illuminates the 26-m paraboloid. Fifty-eight of these expansion coefficients were determined for each X-band horn pattern, and 45 coefficients determined for the S-band horn pattern. The resulting scatter patterns are shown in Figs. 5, 6, and 7. The result of an unequal E and H horn pattern is noted in Fig. 5 since the scattered E and H plane patterns are also unequal.

Also it is apparent that the DSS 13 vertex plate was not designed for X-band. Geometric shadowing by the subreflector extends to about 8 deg. From Figs. 5 and 6 it is noted that this vertex plate achieves its purpose to about 13 to 15 deg, wasting a significant part of the inner paraboloidal region.

Next, the efficiency of these patterns is calculated as illuminators of the 26-m paraboloid. Values are tabulated in Table 1. Observe that these totals do not include spar blockage or surface tolerance. These are not a function of the X-S feed unit.

It is interesting to understand qualitatively the reasons for the slight differences in efficiencies at the various frequencies. The horn patterns (Figs. 2, 3, and 4) show the angle of 32.7 degrees, which is subtended by the total subreflector, thus representing the total portion of each pattern that is intercepted. The first item noted is the greater spillover at S-band than at X-band. The reason is evident when looking at these radiation patterns: the S-band pattern is triangular in shape, reaching the −40 dB level at nearly 36 deg, while X-band patterns have much steeper sides (slopes) and reach −40 dB at a smaller angle. Thus a greater fractional energy is intercepted at X-band. Next is noted the differences in illumination efficiency. The superiority of S-band can be noted in Figs. 5, 6, and 7. In this case, the large X-band hole due to the vertex plate has drastically reduced the effectiveness of the reflector area compared to S-band. The superiority of 8.425 GHz illumination efficiency over 7.175 GHz can be seen in Figs. 5 and 6. The taper at 7.175 GHz (Fig. 6) can be seen as greater than 8.425 GHz (Fig. 5), the result of the greater taper on the hyperbola intercept (−16 dB, Fig. 3) compared to −14 dB at 8.425 GHz (Fig. 2). Also, phase efficiency is superior at S-band, again the effect of the vertex plate having the more serious effect at the shorter wavelengths. It becomes apparent that the subreflector could be redesigned for this antenna, if one desired further X-band improvement, to increase illumination and phase efficiency by, perhaps, a total of 5 percent.

III. The Feedcone

The new X-S feedhorn and other necessary equipment (power lines, brackets to hold masers and other electronic gear, etc.) were installed in a feedcone at JPL. The completed unit is shown in Fig. 8. This assembly was sent to DSS 13 for further measurement and installation on the 26-m antenna.

Figure 9 is a photograph of this new installation at DSS 13 and Fig. 10 depicts the older reflex feed as applied to the 34-m modifications.

The plan to evaluate the common aperture X-S horn, as installed in a feedcone system at DSS 13, was to measure total operating system noise temperature (T_{op}) in a normal feedcone-on-ground test mode followed by T_{op} (feedcone antenna mounted) and 26-m antenna area efficiency (η) measurements. Two fundamental problems have prevented the gathering of reliable data.

First, the cone-on-ground S-band measurements are clouded by a problem discovered after the feedcone was antenna mounted. Although JPL Mesa Antenna Range measurements at S-band were done with a proper assembly of the feedhorn yoke assembly (power division for phasing the four S-band horn inputs), an inadvertent reassembly within the feedcone introduced a phasing problem. Resultant 26-m antenna main beam initial measurements showed a highly squinted and elliptical beam prior to proper assembly of the yoke. Thus full confidence was not obtained in the present S-band T_{op} (23 K) since the expected 3 K feedcone OFF/ON antenna value (due to spillover and scatter) has not been demonstrated. The approximate S-band area efficiency under these uncertain conditions is 62 percent.

Secondly, initial feedcone-on-ground X-band T_{op} measurements appeared high (21 K) and not stable. Later, with the feedcone antenna mounted, the measurements were very high (about 30 to 40 K) and very unstable. Additionally, different

T_{op} measurement schemes produced different results. The problem was traced to the X-band TWM, an old unit that suffered from years of thermal cycling. The travelling wave comb structure had become distorted and short circuited in places. Now repaired and reinstalled in the antenna-mounted feedcone, different measurement schemes all indicate T_{op} in the low 20 K class. During the period with a suspect maser, X-band antenna efficiency appeared to be 48 percent. This value now requires another evaluation.

In summary, despite the above problems, the X-S common aperture horn (initial receive-only model) appears to have no major problems; a full evaluation is planned just prior to (and after) the next opportunity for feedcone removal from the 26-m antenna. At that time, feedcone-on-ground T_{op} measurements will be carefully compared with feedcone-on-antenna T_{op} measurements to discern the expected spillover and scatter contributions.

IV. Further Horn Study, Second Generation

The X-band horn has exhibited evidence of an operational problem as noted in the unequal E and H plane patterns of Fig. 2. There appears to be some small amount of moding, i.e., the generation of other corrugated hybrid modes than the desired HE_{11} mode. For instance, the EH_{11} mode may be generated at low X-band when input grooves are less than $\lambda/4$, or higher modes, the HE_{12} and EH_{12}, when the horn is sufficiently large and horn interruptions (discontinuities) may occur. It was not obvious what caused these problems.

Toward the end of solving this problem, several tests were made using segments of the full-scale horn that were left over from the first model development. An X-band input section was available, to about 12.7-cm (5-inch) aperture, and an additional section was built for enlarging the sample and to allow various tests to be made. Also, an additional input piece was made for the X-band, which consisted of a gradual radius change from the X-band cylindrical guide to the 17.1-deg horn flare instead of the abrupt 17.1-deg horn attached to cylindrical waveguide.

Basically, the following tests were made:

(1) Metallic taping off two grooves to simulate the combiner input that results in the pitch change for the corrugations.

(2) Building the additional section at a different flare angle to simulate the change of flare angle for this horn.

(3) Using the gradual flare change at the X-band input.

The following results were noted:

(1) A significant (very noticeable) change occurs when the gradual taper is used. The abrupt change from cylindrical to the 17.1-deg flare is a major cause of moding.

(2) Neither the small flare angle change nor the corrugation interruption caused a significant moding, although some was noticed.

The conclusion was that a new horn will be constructed using the gradual change to the 17.1-deg flare, over about a 10.2-cm (4-inch) transition length. Further investigation into the optimum groove depth and corrugation pitch is being carried on.

Also in this second-generation study, a new diplexer/combiner must be developed so that the S-band system will have sufficient bandwidth for transmission as well as low noise reception. Although the first generation diplexer (now at DSS 13) offered sufficient X-band isolation (Ref. 2), it had an operating bandwidth of less than 100 MHz in S-band. The second-generation diplexer being designed will use the same approach as the first-generation design, except that the radial transmission line for S-band injection will be about 70 percent wider to obtain the bandwidth, and the X-band radial line chokes will be increased from 2 to 6 in number to maintain the high X-band isolation.

References

1. W. F. Williams, "A Prototype DSN X-S Band Feed: DSS 13 First Status Application," *DSN Progress Report 42-44*, Jet Propulsion Laboratory, Pasadena, Calif., Jan.-Feb. 1978.

2. W. F. Williams, "A Prototype DSN X-S Band Feed DSS 13 Application Status (Second Report)," *DSN Progress Report 42-47*, Jet Propulsion Laboratory, Pasadena, Calif., July-Aug. 1978.

3. Arthur C. Ludwig, "Calculations of Scattered Patterns from Asymmetrical Reflectors," Technical Report 32-1430, Jet Propulsion Laboratory, Pasadena, Calif., Feb. 15, 1970.

Table 1. Total efficiency as a function of frequency

Efficiency Type	Frequency		
	8425 GHz	7175 GHz	2295 GHz
Total spillover	0.96660	0.97139	0.88693
Illumination	0.86173	0.82389	0.88610
Cross-polarization	0.98861	0.99430	0.99590
Phase	0.89627	0.89301	0.92438
Blockage (subreflector	1.0000	1.0000	0.96900
Totals	0.73804	0.70687	0.70107

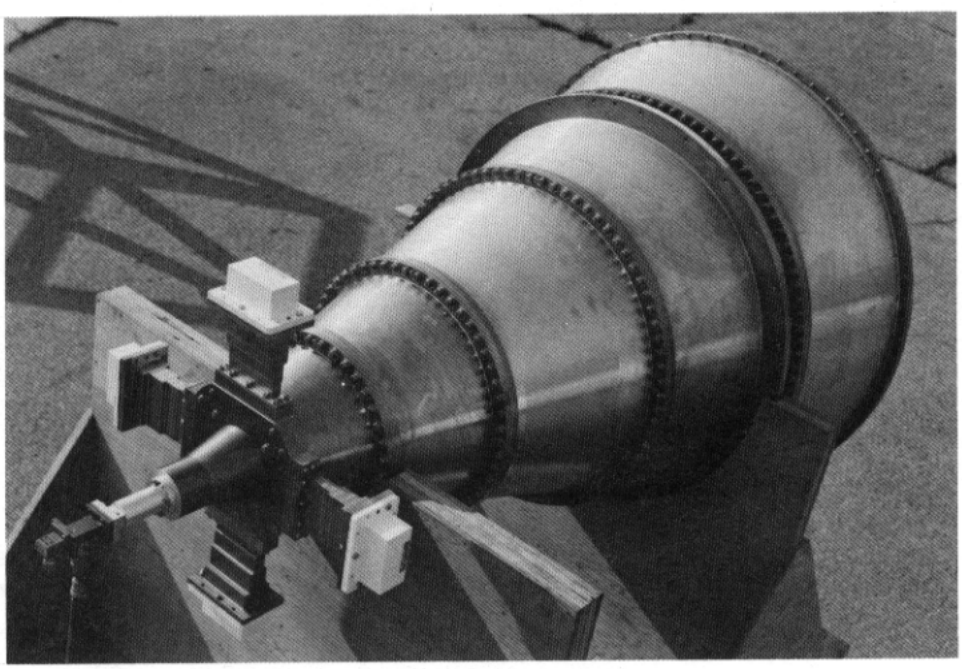

Fig. 1. Final first-generation X-S horn

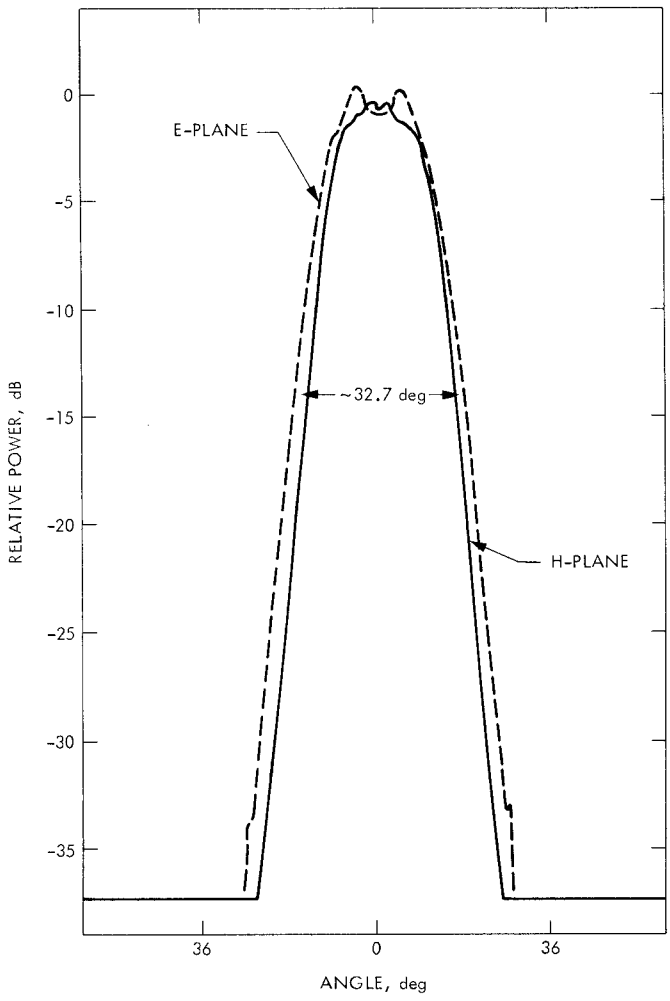

Fig. 2. Final X-S horn pattern at f = 8.425 GHz linear polarization

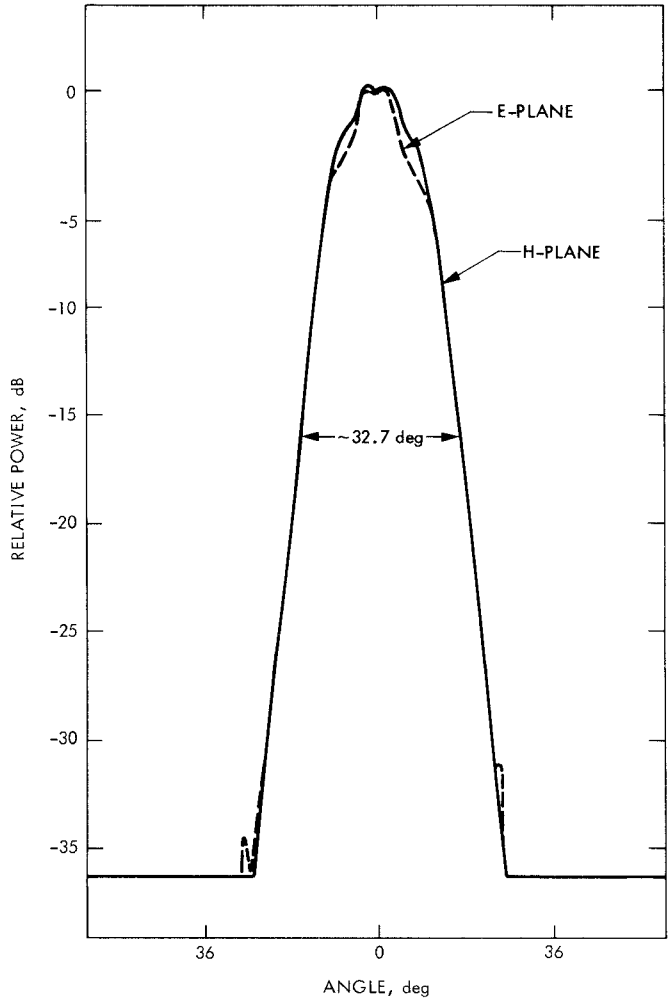

Fig. 3. Final X-S horn pattern at f = 7.175 GHz linear polarization

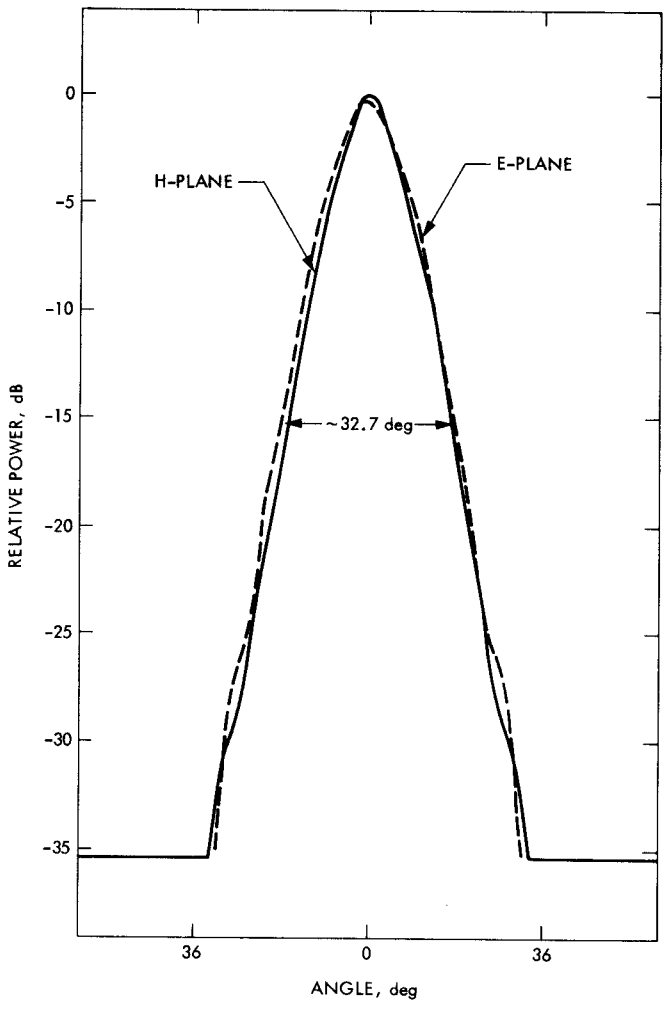

Fig. 4. Final X-S horn pattern at f = 2.295 GHz linear polarization

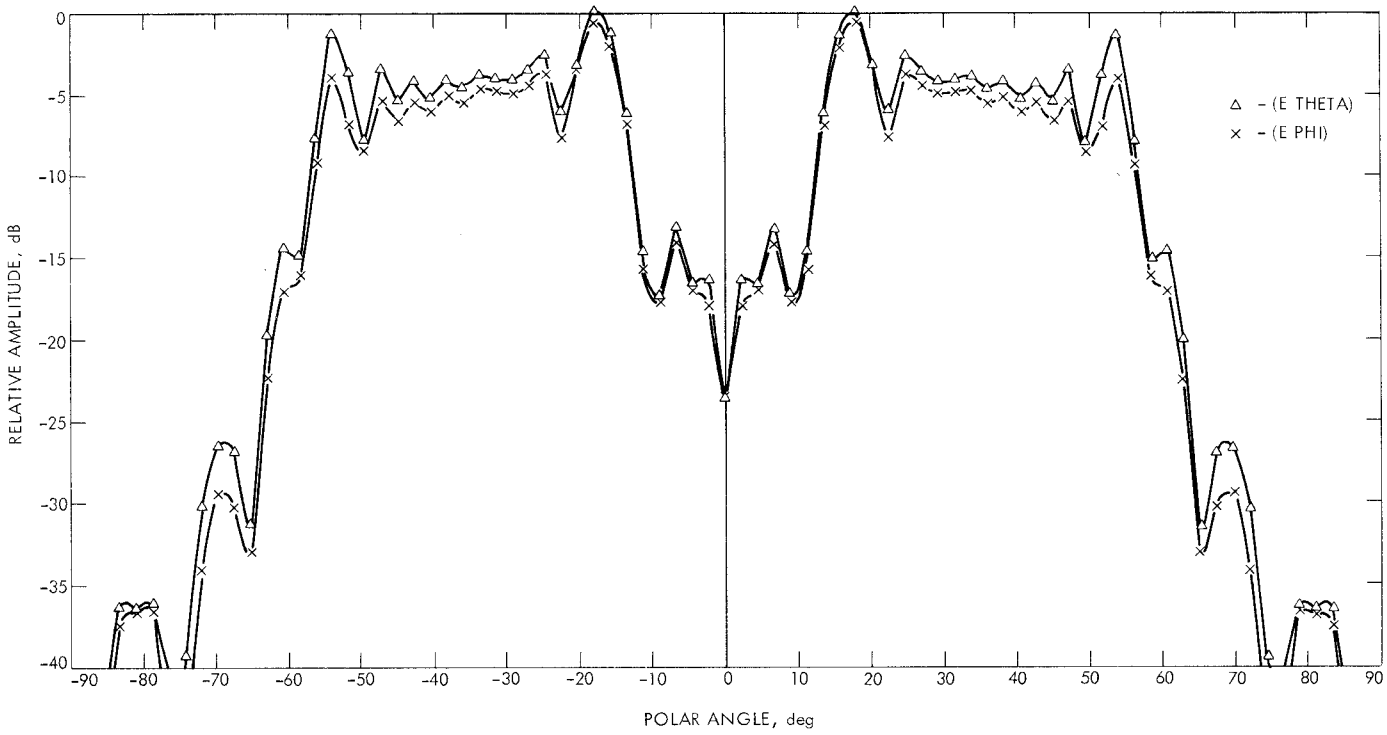

Fig. 5. The 8.425 measured amplitude pattern, 58 modes scattered from DSS 13 subreflector

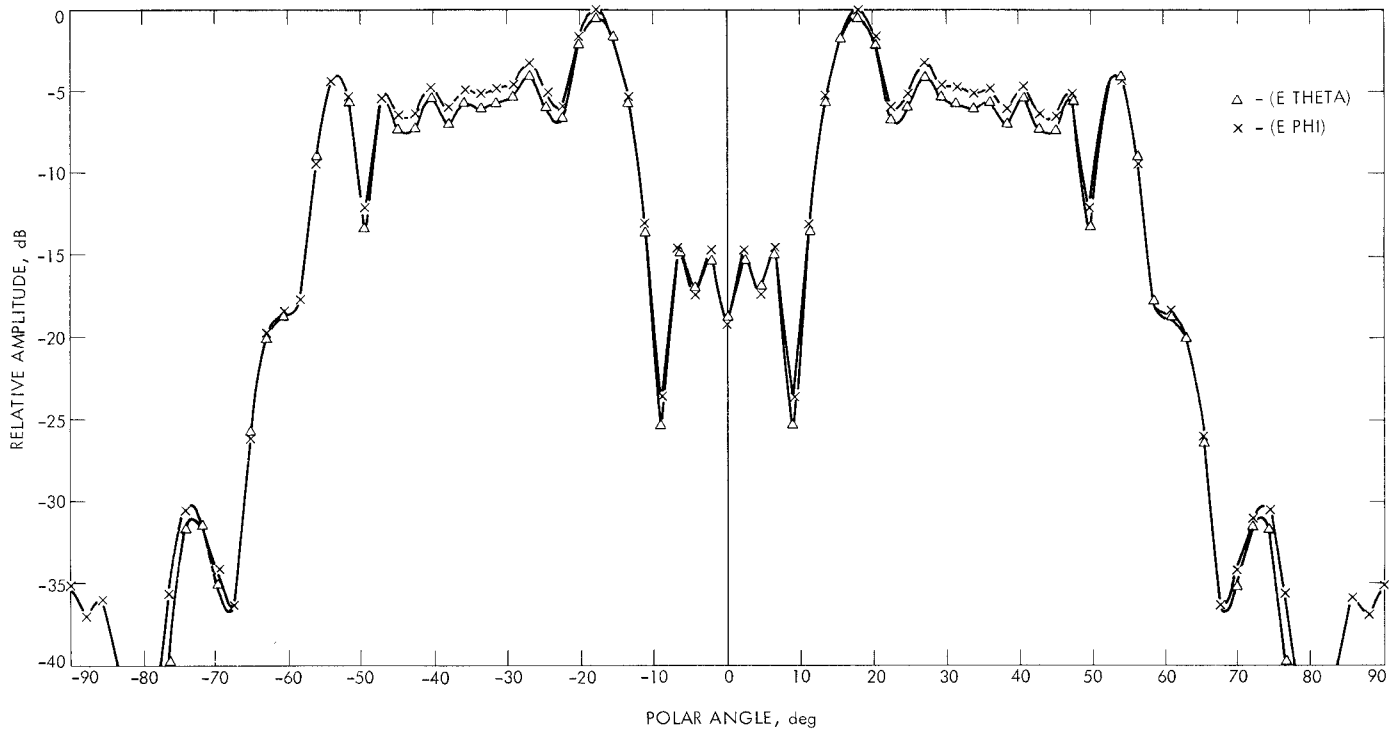

Fig. 6. The 7.175 measured amplitude pattern, 58 modes scattered from DSS 13 subreflector

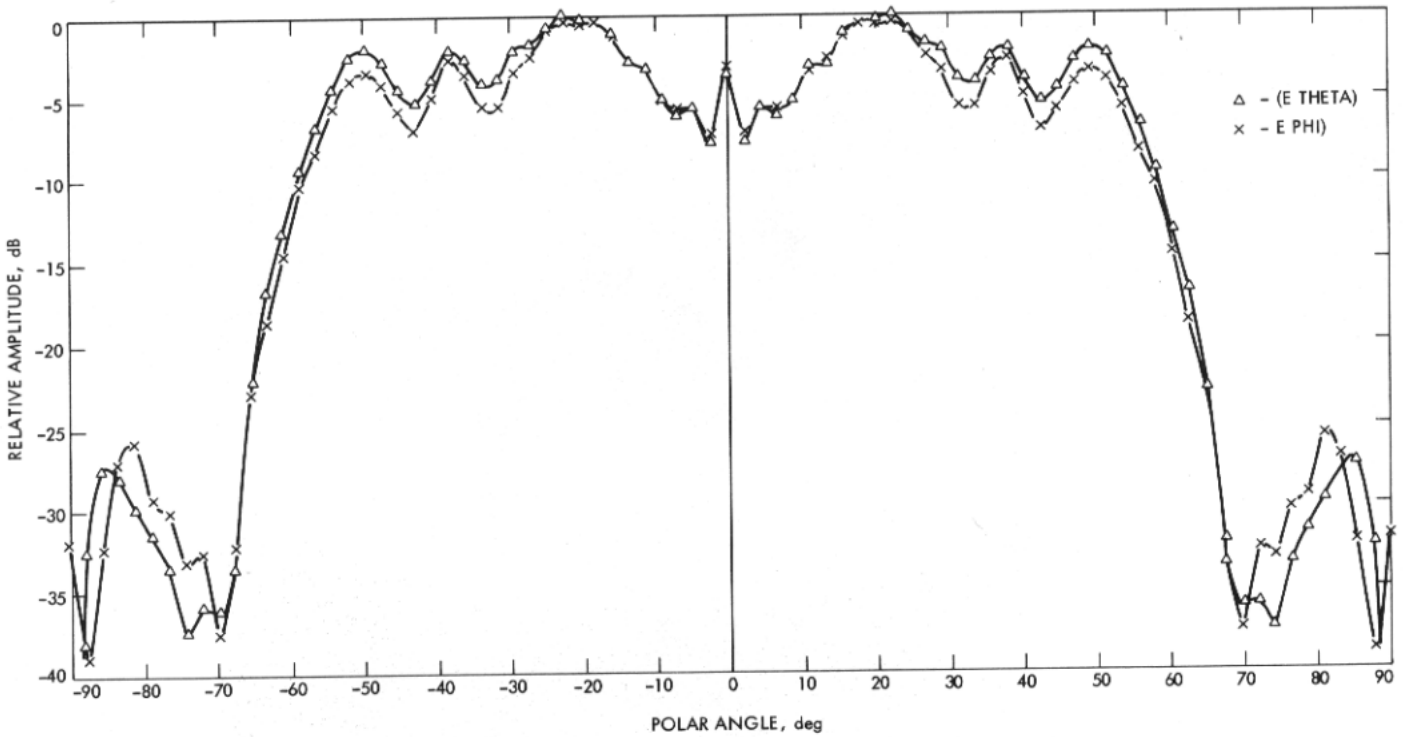

Fig. 7. The final 2.295 measured patterns, 45 modes, scattered from DSS 13 subreflector

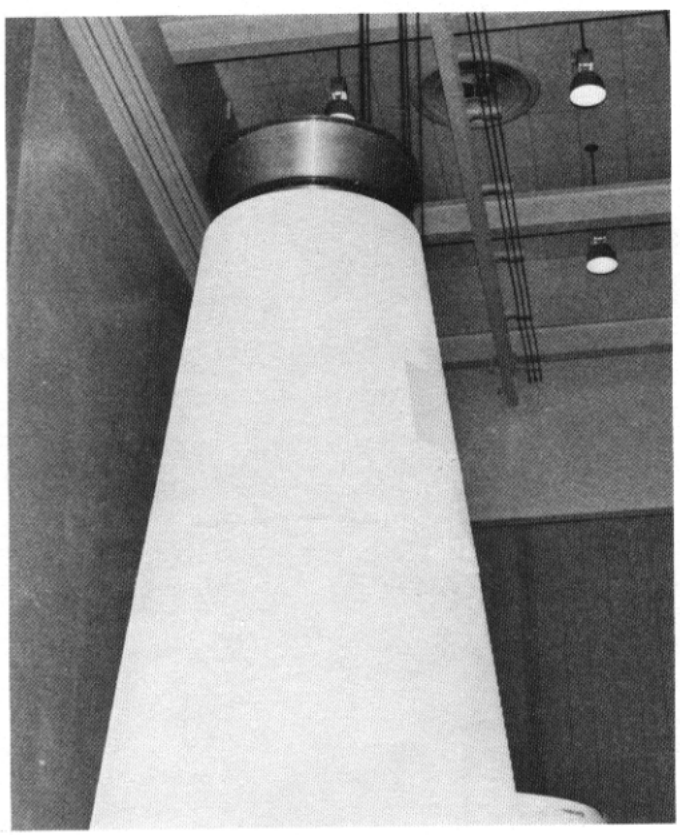

Fig. 8. First generation S-X feed mounted in its feedcone

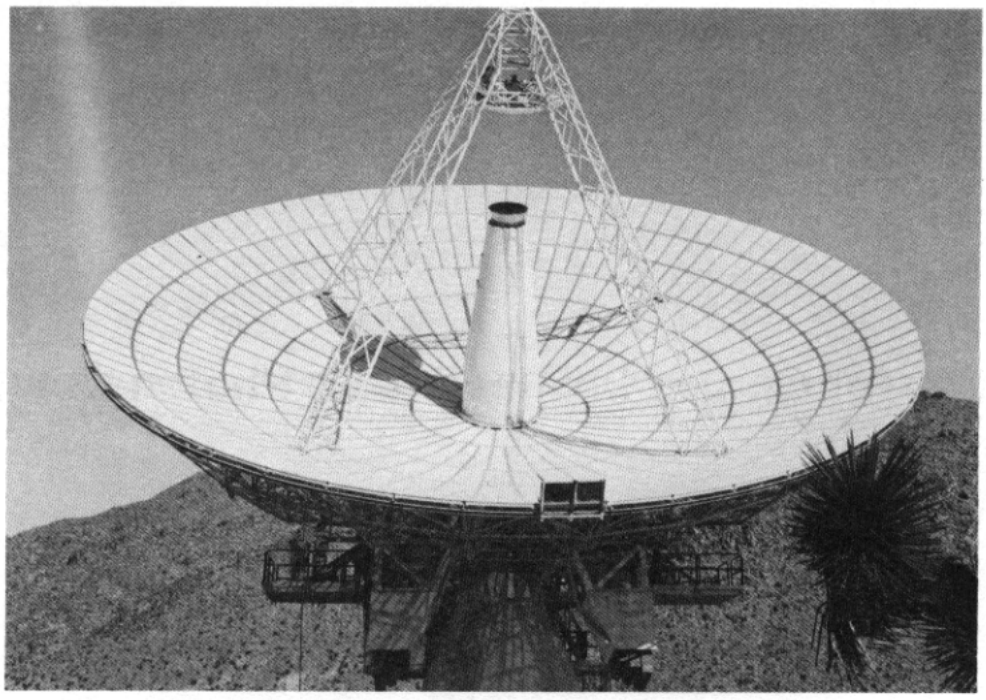

Fig. 9. The first-generation X-S horn at DSS 13

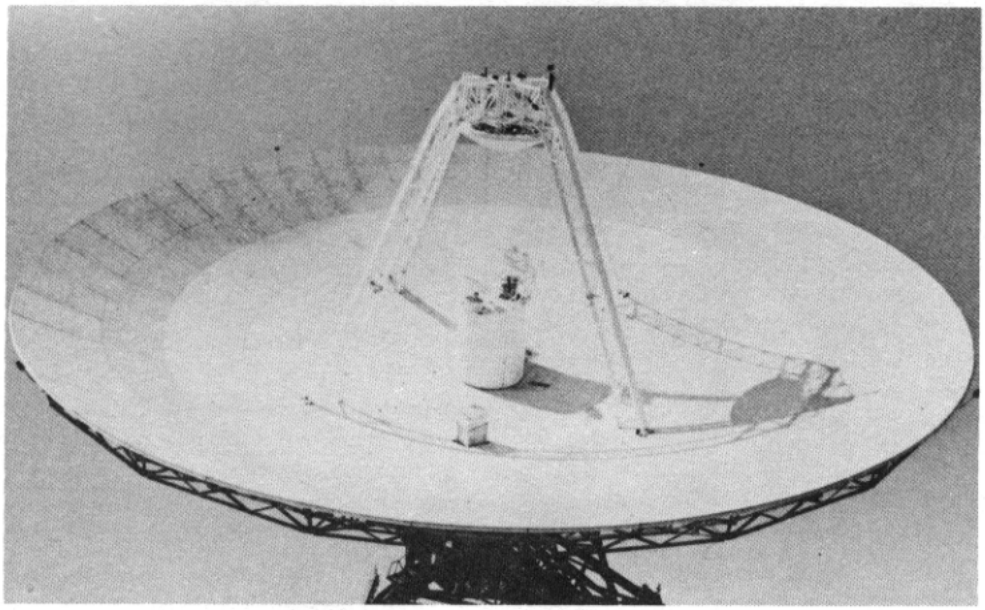

Fig. 10. The S-X reflex feed on the 34-m antenna